Journal of High Energy Physics, Gravitation and Cosmology, 2026, 12(2), 839-856
https://www.scirp.org/journal/jhepgc
ISSN Online: 2380-4335
ISSN Print: 2380-4327

Beyond the Causal Diamond: A Probabilistic Model of Cyclical Quantum Gravity

George Davey

Independent Researcher, West Des Moines, IA, USA
Email: George.Davey@QuantumLinear.com

How to cite this paper: Davey, G. (2026) Beyond the Causal Diamond: A Probabilistic Model of Cyclical Quantum Gravity. *Journal of High Energy Physics, Gravitation and Cosmology*, **12**, 839-856.
https://doi.org/10.4236/jhepgc.2026.122045

Received: December 12, 2025
Accepted: March 28, 2026
Published: March 31, 2026

Abstract

We propose a finite, probabilistic, and algebraic formulation of quantum gravity based on the **Chrono-Emergence (CE)** emergence law and the **Discrete-State Time Density (DTD)** field $\hat{t}$. This framework reinterprets gravity as being driven by elastic strain in the $\hat{t}$ field. We derive a finite critical time density, $\hat{t}_{\text{crit}} = 2\pi/c$, at which spacetime enters a dense-time phase, suppressing coherent wave transport and black body radiation. This mechanism defines the **Chrono-Quantum Mirror (CQM)**, a finite phase boundary that replaces the classical event horizon and supplants the evaporation paradigm. We define the **Timeon Lattice Potential (TLP)** and the **Chrono-Emergent Tunneling (CET)** mechanism as the microscopic drivers for matter-confinement within this field. Cosmologically, we propose a **multiverse lattice** of interacting domains, where the **Lattice Gravitational Strain (LGS)** from causal bleed manifests as dark matter, and the expansionary momentum from a cyclical **Chrono-Shear Event** manifests as dark energy. This cycle culminates in a final, acausal deconfinement and reconvergence of matter-energy that seeds the next domain's *causal onset phase*. We propose distinct, falsifiable experiments to test the theory. The result is a unitary, thermodynamically closed, and observationally-grounded ecosystem of solutions for foundational physics termed **Timeon Lattice Multiverse Cosmology**.

Keywords

Quantum Gravity, Time-Density Field, Black Hole Thermodynamics, Causal Diamonds, Cyclical Cosmology

1. Introduction

Quantum gravity requires finiteness, causality, and algebraic closure. We construct a framework combining: (1) Chrono-Emergence (CE) with constant $\tilde{K}$

enabling **spontaneous emergence** from true nothingness over extreme timescales, formerly known as DAGE (Density-Activated Graduated Emergence) [1]; (2) Discrete-State Time Density (DTD), a scalar $\hat{t}$ encoding time-density whose phase structure governs both emergence and radiative behavior; and (3) a finite-diamond operator algebra with edge-mode augmentation and holographic log caps. Standard approaches often remain either divergent or dependent on extrinsic mathematical extensions (see, e.g., [2]). All large regulators enter only via $\{\ln R_{\max}, \ln T_{\max}\}$; explicit 2^{Q} never appears. The resulting log-safe operator theory preserves gauge closure and unitarity while matching Kerr and cosmological observables.

This framework is built on a re-interpretation of spacetime itself, formally defining a time-density field $\hat{t}$ as the primary driver of gravity. We derive a finite critical threshold for this field, which defines the physics of black holes and provides the mechanism for a cyclical, timeon lattice **(T-Lattice)** multiverse cosmology, which in turn explains the phenomena of dark matter and dark energy. We conclude by proposing specific experimental tests for this new architecture.

Finally, we distinguish two operational stages of Chrono-Emergence. The first is the primordial generation of the time-density field—and hence spacetime—from true nothingness over super-aeon scales. The second is the structural organization of this lattice into the stable structures we identify as Matter. This distinction frames our technical use of the term *acausal*: it denotes a transient regime (such as the transition between these stages or during a Chrono-Shear Event) wherein the lattice undergoes phase reconfiguration, preventing a single global causal foliation while preserving local conservation. Consequently, matter is not defined as a substance distinct from the manifold, but as the Timeon Lattice itself, reorganized into stable, localized configurations.

2. Theoretical Foundations

2.1. CE Emergence and the DTD Field

Let $\hat{t}(x)$ be the Discrete-State Time Density (DTD) scalar, which occupies discrete phases. Empirically accessible phases include the **vacuum phase** ($\hat{t}_1$), in which spacetime behaves as a superfluid supporting the frictionless propagation of electromagnaetic waves and gravitational fields; the **atomic phase** ($\hat{t}_a$), in which mutual confinement forms a complex topology and generates stable matter; and the **dense phase** ($\hat{t}_2$), which corresponds to the interior of a black hole where coherent wave transport and black body radiation become nearly unsupported and strongly redshifted once $\hat{t}$ exceeds a critical threshold (derived in Section IV). A transient **shear phase** ($\hat{t}_3$), appears at the end of a cosmic cycle; its reconvergence seeds the next domain's *causal onset phase*.

Let $F(\hat{t}) = C\hat{t}^{\alpha}$ be the fertility field with $\alpha > 0$. An emergence source enters the matter sector as

$$\nabla_{\mu} T^{\mu\nu}_{\text{mat}} = \frac{\tilde{K}}{c^2} u^{\nu} F(\hat{t}). \tag{1}$$

The scalar $\hat{t}$ therefore has multiple simultaneous roles: it enhances CE fertility, stabilizes the atomic phase structure, and drives spacetime into the dense-time phase where extended wave support and Planck-equilibrated emission both become nearly unsupported.

2.2. Finite-Diamond Postulates (P1-P10)

P1 finite emergence; P2 time-density phase modulation; P3 wave-support cutoff for large $\hat{t}$: beyond a finite critical time density $\hat{t}_{\text{crit}}$, the medium enters the dense-time phase and cannot physically support extended vacuum-phase quantum information, interference, tunneling, or black body equilibration; P4 mirror first law; P5 fertility-curvature coupling; P6 backreaction $G_{\mu\nu} = 8\pi G\left(\langle T_{\mu\nu}\rangle + T_{\mu\nu}^{\text{CE}}\right)$; P7 exterior recovery; P8 Petz criterion; P9 local GSL; P10 finite-universe normalization $\int \tilde{K} F \mathrm{d}V \mathrm{d}t = \zeta M_U c^2$, $0 < \zeta < 1$.

2.3. Finite Causal Diamonds and Log Caps

All observables live on a finite causal diamond $\mathcal{D}$ with corner $\mathcal{C} = \partial\Sigma$. The holographic entropy cap is

$$\ln S_{\max} = \ln \pi + 2 \ln R_{\max} - 2 \ln \ell_P, \tag{2}$$

and large scales appear only via logs.

3. The Time-Density Field as the Dominant Component of Spacetime Curvature

Classical general relativity interprets gravity as curvature of spacetime produced by mass-energy. However, all empirical signatures of curvature—gravitational redshift, time dilation, and signal delay—are temporal in nature. No direct measurement of intrinsic spatial curvature, independent of clock-rate variation, has yet been performed. This motivates an interpretation in which the empirical signatures of gravity are *dominated* by the *condensation of time*: a spatial gradient in the density of proper time.

3.1. The Time-Density Field

Classical general relativity treats the metric $g_{\mu\nu}$ as the primary physical field. However, within the Timeon Lattice framework, we invert this causal hierarchy. We postulate that the metric is an emergent description of the underlying Time Density field $\hat{t}$.

We formalize this by defining $\hat{t}$ analogously to an optical refractive index. Just as a dielectric medium with a high refractive index slows the phase velocity of light ($v = c/n$), a region of high Time Density slows the flow of proper time relative to asymptotic coordinate time. In this view, the "curvature" of spacetime is the refractive response to gradients in the time density.

Operational units

We interpret the time-density scalar $\hat{t}$ operationally as *proper time per unit*

proper length,

$$\hat{t} \equiv \frac{\mathrm{d}\tau}{\mathrm{d}l}, \tag{3}$$

with units $\left[\hat{t}\right] = \mathrm{s}\cdot\mathrm{m}^{-1}$. This captures the intended meaning that increasing $\hat{t}$ corresponds to "more time per unit space".

For metric and redshift expressions it is convenient to use a dimensionless lapse-like normalization:

$$n_t \equiv c\hat{t}, \tag{4}$$

so that n_t is dimensionless and $\hat{t} = n_t / c$.

3.2. Relation to the Metric Tensor: The Refractive Postulate

Using the dimensionless normalization $n_t \equiv c\hat{t}$, the local time density is inversely proportional to the gravitational redshift factor (the lapse function). We adopt the **Refractive Postulate**:

$$n_t(r) \equiv \frac{n_{t,\infty}}{\sqrt{-g_{tt}(r)}}, \tag{5}$$

The physical time density is recovered via $\hat{t} = n_t / c$ (with $n_{t,\infty} = c\hat{t}_\infty$).
where $n_{t,\infty}$ is the normalized vacuum time density at infinity (with $n_{t,\infty} = c\hat{t}_\infty$).
For the Schwarzschild solution, where $-g_{tt} = 1 - 2GM/\left(rc^2\right)$, this yields:

$$n_t(r) = n_{t,\infty}\left(1 - \frac{2GM}{rc^2}\right)^{-1/2}. \tag{6}$$

This formulation ensures that as one approaches the horizon ($r \to r_s$), the normalized time density diverges ($n_t \to \infty$), equivalently $\hat{t} \to \infty$. This divergence provides the physical mechanism for the phase transition into the saturated Dense-Time State.

3.3. Quantization of the Time-Density Field and the Timeon

If $\hat{t}$ is fundamental and stores energy, it should support quantized excitations and stable reconfigurations. We identify these discrete excitations as **timeons**—localized quanta of the time-density field. While the vacuum exists in a low-density **stable wave phase**, we postulate that baryonic matter is not a distinct substance, but a **Baryon Partner State (BPS)**: a localized, highly stable configuration where timeons are mutually confined in an **atomic phase**. In this view, mass is defined not as an intrinsic property of a particle, but as the integral of the timeon density trapped within the BPS.

The stability of this state is governed by the **Timeon Lattice Potential (TLP)**, denoted formally as $V\left(\hat{t}\right)$, which separates the vacuum phase from the atomic phase. We model the transition from the vacuum wave phase to the stable BPS configuration via a probabilistic analogous to quantum tunneling observed in laboratory electronics. Just as an electron with a specific energy may escape a higher-potential voltage barrier through a classically forbidden transition [3]—so

too may the time-density field undergo **Chrono-Emergent Tunneling (CET)** over aeon timescales to form stable matter. In this framework, the fertility field $F(\hat{t})$ functions as the macroscopic manifestation of these microscopic lattice transitions, fundamentally coupling the emergence rate to the time-density phase state of the manifold. This phase transition defines the dual functional roles of the timeon within the T-Lattice architecture:

The Passive Role (Gravity). The Baryon Partner State (mass) creates a localized spike in time density. This exerts a radial tension on the surrounding vacuum lattice. For an isolated BPS, this strain propagates isotropically, resulting in zero net motion. However, when a second BPS enters this field, the strain symmetry is broken. The lattice region between the bodies becomes saturated with shared tension, while the exterior vacuum pull remains unopposed. Gravity is the resultant **elastic restoration force** driving the bodies together to resolve this pressure asymmetry.

The Active Role (Catalyst). The timeon acts as the fundamental broker of matter-energy equivalence. In high-energy events such as particle-antiparticle annihilation, the confining geometry of the BPS is disrupted. The timeons locked in the atomic phase are released back into the vacuum wave phase. This phase transition catalyzes the conversion of the "frozen" potential energy of the BPS into the kinetic propagation of pure energy. This provides a direct physical mechanism for $E = mc^2$ rooted in Timeon Lattice Cosmology: E is the kinetic phase of the timeon, while m is the confined phase.

4. The DTD Phase Boundary: Waveform Suppression and the CQM

The DTD field's phase structure is governed by a finite causal-bandwidth limit.

4.1. Quantum Coherence Constraint

For a quantum field, spatial coherence requires that phase information can propagate across at least one Compton wavelength, $\lambda_C = \hbar/(mc)$, within approximately one intrinsic rest-phase period, $T_0 = 2\pi\hbar/(mc^2)$. Demanding that causal influence can carry phase across λ_C during T_0 gives a lower bound on the effective signaling speed for that field,

$$v_{\text{eff}} \gtrsim \frac{\lambda_C}{T_0} = \frac{c}{2\pi}. \tag{7}$$

If a region enforces v_{eff} below this threshold, interference, tunneling, and delocalized eigenstates become operationally impossible. The wave cannot act like a wave.

4.2. Critical Time Density $\hat{t}_{\text{crit}}$

From the perspective of an external observer, the inferred time-per-length of causal transport is $\hat{t}_{\text{obs}} \equiv \mathrm{d}t_{\text{out}}/\mathrm{d}\ell = 1/v_{\text{eff}}$. Recalculating Equation (7) yields a uni-

versal mass-independent upper bound on viable wave transport,

$$\hat{t}_{\text{crit}} \equiv \hat{t}_{\text{obs}}\big|_{v_{\text{eff}}=c/(2\pi)} = \frac{2\pi}{c} \approx 2\times 10^{-8}\,\text{s}\cdot\text{m}^{-1}. \tag{8}$$

This defines a finite time-density phase boundary:

$$\hat{t} > \hat{t}_{\text{crit}} \;\Rightarrow\; \text{Wave propagation nearly unsupported (dense-time phase)}. \tag{9}$$

Beyond this point, quantum fields cannot maintain spatially extended coherence on their own internal timescales. Information dependent on waves or propagated by waves is suppressed.

4.3. Suppression of Blackbody Radiation

A conventional Planck spectrum assumes that modes repeatedly exchange energy and approach thermal occupation. If v_{eff} is suppressed below $c/(2\pi)$, even near-lightlike excitations cannot traverse macroscopic distances quickly enough to equilibrate. Thermal radiation cannot self-average into a smooth blackbody field. The domain cannot build or sustain a Planck spectrum recognizable to an external observer; radiative cooling stalls, and the region appears radiatively dark. We call this *black body failure*.

5. Edge-Mode Symplectic Augmentation

5.1. Presymplectic Form with Conserved, Causal Bleed

$$\tilde{\Omega}_{\text{edge}} = \oint_{\mathcal{C}} \left(\delta q_A \wedge \delta p^A + \mathcal{R}\left(\chi;\epsilon,\Xi_1,\Xi_2\right)\delta q_A \wedge \delta p^A_{\text{bleed}} \right), \tag{10}$$

with regulator

$$\begin{aligned} &\mathcal{R}\left(\chi;\epsilon,\Xi_1,\Xi_2\right) = \mathrm{e}^{-\epsilon g(\Delta\chi)}\Theta\left(1-\Xi_1\right)\Theta\left(1-\Xi_2\right), \\ &\epsilon = 10^{-\epsilon},\ \Xi_1 = \frac{L_{\text{bleed}}}{R_{\max}} \ll 1,\ \Xi_2 = H\tau_{\text{bleed}} \lesssim 1. \end{aligned} \tag{11}$$

5.2. Holographic Commutator Suppression

$$\left[\hat{q}_A(\theta), \hat{p}^B(\theta')\right] = i\delta_A^B \delta(\theta-\theta')\mathrm{e}^{-\Delta S_{\text{cap}}},\ \Delta S_{\text{cap}} = \max\left(0, S_{\text{edge}} - S_{\max}\right). \tag{12}$$

5.3. Closure

At fixed $\left(\ln R_{\max}, \ln T_{\max}\right)$ the total symplectic variation vanishes, $\delta\Omega_{\text{bulk}} + \delta\tilde{\Omega}_{\text{edge}} = 0$, ensuring gauge closure and causality.

6. CE/DTD Dynamics and the Mirror First Law

$$H_{\text{edge}}[F] = \frac{\tilde{K}}{c^2} FA[\mathcal{C}] + H_0,\ A[\mathcal{C}] = \oint_{\mathcal{C}} \sqrt{\gamma}\,\mathrm{d}^2\theta. \tag{13}$$

A fertility variation at fixed logs gives

$$\delta Q_F = \iota_{\delta_F}\tilde{\Omega}_{\text{edge}} = \delta H_{\text{edge}}[F] = \frac{\tilde{K}}{c^2}\delta FA. \tag{14}$$

The charge is central: $\{Q_F, A\} = \{Q_F, \Xi(\hat{t})\} = \{Q_F, Z(\omega)\} = 0$.

7. Information Theory and Thermodynamic Consistency

7.1. Petz Sufficiency (P8)

For Gaussian code $\mathcal{C}$ and channel Φ with dephase γ_b, the recovery map [4]

$$\mathcal{R}_\sigma(X) = \sigma^{1/2}\Phi^\dagger\left[\Phi(\sigma)^{-1/2} X \Phi(\sigma)^{-1/2}\right]\sigma^{1/2} \tag{15}$$

recovers the input if and only if $S(\rho\|\sigma) = S(\Phi\rho\|\Phi\sigma)$. In the presence of small dephasing, fidelity expands as

$$\bar{\mathcal{F}}(\Delta F, \gamma_b) \geq 1 - c_1\gamma_b - c_2(\Delta F)^{-2} \tag{16}$$

hence $F \geq 0.98$ when $\Delta F \geq \Delta F(\gamma_b, \tilde{K})$.

7.2. Local Generalized Second Law (P9)

On a null cut $\mathcal{N}$,

$$\frac{\mathrm{d}S_{\mathrm{gen}}}{\mathrm{d}u} = \frac{\mathrm{d}S_{\mathrm{bulk}}}{\mathrm{d}u} + \frac{\mathrm{d}S_{\mathrm{edge}}}{\mathrm{d}u} \geq 0, \tag{17}$$

for causal kernel K with $\Xi_1 \ll 1$, $\Xi_2 \lesssim 1$ and $\partial_{\hat{t}} \ln F \leq 2\pi/\kappa_{\mathrm{eff}}$.

7.3. Unified Thermodynamic Statement

$$\boxed{\delta Q_F = \frac{\tilde{K}}{c^2}\delta F A \;\Leftrightarrow\; \delta S_{\mathrm{gen}} = \frac{\delta Q_F}{T_{\mathrm{eff}}},\; T_{\mathrm{eff}}^{-1} = \frac{2\pi}{\kappa_{\mathrm{eff}}}.} \tag{18}$$

Thus, fertility variation plays the same role as temperature in standard thermodynamics, completing the unification of energy, entropy, and information in the CE/DTD framework, echoing ideas connecting gravity and thermodynamics [5]. In regions where $\hat{t} > \hat{t}_{\mathrm{crit}}$, radiative channels close and δQ_F is retained locally. This is the same black body failure enforced by the CQM.

8. Kerr Calibration: The Chrono-Quantum Mirror (CQM)

8.1. Pöschl-Teller Mapping and the CQM

$$V_{\mathrm{PT}}(x) = \frac{V_0}{\cosh^2\left[a\left(x - x_p\right)\right]},\; \omega_{\mathrm{PT}} = \sqrt{V_0 - a^2/4} - i\frac{a}{2}, \tag{19}$$

matched to Kerr quasinormal modes (QNMs) by $a = 2\left|\mathrm{Im}\,\omega_{lm0}\right|$, $V_0 = \left(\mathrm{Re}\,\omega_{lm0}\right)^2 + \left(\mathrm{Im}\,\omega_{lm0}\right)^2$ [6]. This model replaces the classical event horizon with a Chrono-Quantum Mirror (CQM) at the stretched horizon $r_s = r_+(1+\varepsilon)$. The CQM is the *finite time-density phase boundary* at $\hat{t}_{\mathrm{crit}} = 2\pi/c$, where the DTD field enters the dense-time phase (as derived in Section IV). Across this boundary, the medium scarcely supports coherent quantum wave transport or Planck-equilibrated black body emission. Phase information cannot propagate into the high-$\hat{t}$ interior, and all radiative channels are quenched.

Relation to apparent-horizon models

Recent work by Vaz [7] and by Corda [8] has emphasized that the classical event horizon is not a fundamental geometric entity, but rather an apparent, dynamical

surface emerging from quantum collapse dynamics at the Schwarzschild scale. The Chrono-Quantum Mirror is fully compatible with this conclusion. In the present framework, the apparent horizon arises as a sharp, state-dependent phase boundary in the time-density field, reached under extreme gravitational strain and extended dwell time, where wave-supported transport diminishes. The CQM therefore does not represent a confining surface or information trap, but an emergent boundary beyond which the local laws governing wave propagation and equilibration change. From an exterior viewpoint, this produces observational blackness and radiative quiescence without requiring a classical event horizon, while preserving strong gravity and allowing the boundary location to shift dynamically with accretion and mergers.

Near the would-be horizon r_+, $r \approx (1/2\kappa)\ln(r - r_+)$ and for r_s:

$$L \approx L_0 + \frac{1}{2\kappa}\ln\frac{1}{\varepsilon},\ \Delta t_{\text{echo}} = 2L. \tag{20}$$

8.2. No-Echo and Superradiance-Quench Bounds

$$\begin{aligned} &G(\omega) = \sqrt{R_{\text{bar}}(\omega)R_{\text{bnd}}(\omega)}\,\mathrm{e}^{-\alpha(L,\omega)} < 10^{-3}, \\ &R_{\text{bnd}}(\omega) < 10^{-6}\mathrm{e}^{2\alpha(L,\omega)}\left[R_{\text{bar}}(\omega)\right]^{-1}. \end{aligned} \tag{21}$$

The CQM, by enforcing the dense-time phase, provides the physical mechanism for this no-echo reflective boundary. Low-frequency limit:

$$\lim_{\omega\to 0}\frac{\mathrm{Re}\,\mathcal{R}}{\mathrm{Im}\,\mathcal{R}} \to 0,\ \mathcal{R} = \frac{Z_{\text{ext}} - Z}{Z_{\text{ext}} + Z}, \tag{22}$$

reproducing Kerr Love numbers and tidal heating.

9. Cosmology: The Multiverse Lattice

The *Multiverse Lattice* model extends conventional cosmology by proposing that our universe is one of many interacting domains embedded within a larger quasi-causal continuum. Each domain functions as an internally deterministic system, yet the lattice as a whole supports acausal Chrono-Shear events. In this framework, the multiverse lattice is **quasi-causal**: locally governed by consistent physical laws within each domain and locally restarted by acausal origins.

9.1. Mass-Energy Bleed and Lattice Gravitational Strain (LGS)

Bleed represents mass-energy transfer between adjacent domains. Bleed-Out (B_o) and Bleed-In (B_i) arise when a domain's expansion or reconvergence drives it out of local equilibrium. The cumulative result of these imbalances observed as the **Lattice Gravitational Strain (LGS)**: a vector field representing the net gravitational pull (or strain) from mass-energy imbalance across the lattice. This LGS is the physical mechanism for the phenomenon observed inside of any local domain as Dark Matter. It is an emergent lattice effect. The LGS vector $\boldsymbol{S}_L$ quantifies the aggregate gravitational bias experienced by an observer. Domains

in bleed equilibrium (in the center of many mature or nearly equal domains) would experience low LGS, while domains near an edge or boundary (like our own) experience a strong, non-zero LGS vector. This predicts that Dark Matter effects should not be perfectly isotropic.

9.2. Lattice Apogee Limit (LAL) and Dark Energy

The **Lattice Apogee Limit (LAL)** defines the escape-velocity equilibrium for a single domain cell. It is reached when the domain's average expansion momentum is halted by the LGS. This framework re-interprets Dark Energy: it is the residual expansionary momentum from the domain's last Chrono-Shear Event (CSE). This expansion is not eternal; it is predicted to halt at the LAL, at which point gravitational reconvergence begins the contraction phase of the cycle.

9.3. Super-Aeon Lifecycle and the Chrono-Shear Event

The CE emergence source term $\tilde{K}$ is posited to be extremely small. The total mass-energy of a cosmological domain is therefore dominated by the slow, steady accumulation from CE in normal spacetime over a **super-aeon timescale,** T_{aeon}.

$$\dot{\rho}_{\text{m}} + 3H\left(\rho_{\text{m}} + p_{\text{m}}\right) = \frac{\tilde{K}}{c^2} F\left(\hat{t}\right). \tag{23}$$

At the end of this super-aeon, inevitable mergers lead to a final, hypermassive black hole ($M \sim 10^{53}$ kg), a scale commensurate with the total estimated mass of the current observable universe. This triggers a **Chrono-Shear Event**:

- **Deconfinement:** The extreme gravity causes a DTD phase transition, smothering the binding geometry and unraveling the topological integrity of the Baryon Partner State.
- **Acausal Phase:** Matter-energy enters a transient acausal state.
- **Reconvergence:** This acausal state is unstable and collapses. Its re-coherence shock upon re-entering normal spacetime nearby is a cataclysmic event that is a Big Bang (or causal onset phase) of the subsequent domain.

The Chrono-Shear Event—conventionally identified as the Big Bang—is a transient phenomenon, lasting only seconds. We posit that this acausal interval corresponds to the **critical saturation** of the time density metric ($\hat{t} \to \hat{t}_3$). In this terminal state, the lattice reaches its maximal compressive capacity (the Shear Phase), forcing the deconfinement of stable matter while simultaneously driving the Chrono-Emergence fertility $F\left(\hat{t}\right)$ to its peak. This amplified production generates a burst of mass-energy that seeds the causal onset phase of the subsequent domain.

9.4. The 16-Domain Lattice Model

To visualize the quasi-causal layout, consider a 4 × 4 grid of domains $D_1, \cdots, D_{16}$ (**Figure 1**).

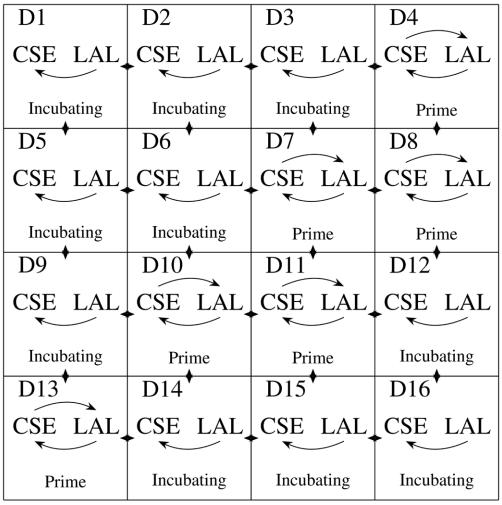

Figure 1. Conceptual schematic of a 16-domain Multiverse Lattice. Each domain (D_1 - D_{16}) follows a cyclic sequence between Chrono-Shear Event (CSE) and Lattice Apogee Limit (LAL). Prime cells (Post CSE) and Incubating cells (No CSE yet) are shown. Bleed arrows (B_o , B_i) denote inter-domain mass-energy flux. The diagram represents one local region of a vastly larger quasi-causal lattice. Domain D7 may resemble our visible universe.

9.5. The Cosmological Black-Hole Lifecycle Signature (CBHLS)

The demographic distribution of black holes within a domain is not static; it evolves deterministically as the domain progresses from its causal onset (Big Bang) toward its Lattice Apogee Limit (LAL). We define the **Cosmological Black-Hole Lifecycle Signature (CBHLS)** as the time-dependent spectral density of black hole mass M and dimensionless spin a_*:

$$\Psi\left(M, a_*; \tau\right) = \frac{\mathrm{d}N}{\mathrm{d}M\mathrm{d}a_*\mathrm{d}V}\left(\tau\right), \tag{24}$$

where τ represents the normalized lattice age of the domain ($0 \le \tau \le 1$). This signature evolves through three distinct phases, allowing an observer to infer the domain's proximity to the Chrono-Shear Event (CSE).

9.5.1. Phase I: The Young Domain ($\tau \ll 0.5$)

In the early expansion phase (post-CSE), the domain is populated by the remnants of the first stellar generations. The signature Ψ is peaked at low masses ($M \sim 10^1$ - $10^2 M_\odot$) with high spin parameters ($a_* \to 1$), reflecting the conservation of angular momentum from energetic progenitor stars.

$$\left\langle M \right\rangle_{\text{young}} \approx M_{\text{stellar}}, \ \left\langle a_* \right\rangle_{\text{young}} \approx 0.8 \text{ - } 0.9. \tag{25}$$

9.5.2. Phase II: The Mature Domain ($\tau \sim 0.5$)

As the domain ages, Chrono-Emergence (CE) adds internal mass, and hierarchical mergers begin to consolidate the population. The spectrum shifts toward intermediate and supermassive scales. Spin distributions broaden and the mean spin decreases, as random-orientation mergers tend to cancel net angular momentum.

$$\frac{\mathrm{d}\langle M\rangle}{\mathrm{d}\tau} > 0 \ \left(\text{Growth}\right), \quad \frac{\mathrm{d}\langle a_*\rangle}{\mathrm{d}\tau} < 0 \ \left(\text{Spin Dilution}\right). \tag{26}$$

We posit our own universe resides in this 'late expansion phase'; we observe a mix of stellar remnants and growing supermassive cores, but the runaway consolidation has not yet begun.

9.5.3. Phase III: The Geriatric Domain ($\tau \to 1$)

As the domain approaches the LAL, the expansion stalls and gravitational reconvergence drives a Runaway Merger Scenario. The population simplifies into a sparse collection of **Hypermassive Black Holes (HMBHs)** ($M \gg 10^{12} M_{\odot}$). Due to the statistical averaging of billions of merger events, the net intrinsic spin of these giants will hedge toward a "Low-Spin" graveyard state:

$$\lim_{\tau \to 1} \Psi \approx \delta\left(M - M_{\mathrm{HMBH}}\right)\delta\left(a_*\right). \tag{27}$$

The detection of such a population—few, clustered, hypermassive, and low-spinning—would sign the domain as distinctively "Geriatric", indicating an imminent Chrono-Shear Event.

9.6. Stochastic Background Inference

The collective gravitational wave emission from these populations generates a stochastic background, $\Omega_{\mathrm{GW}}^{\mathrm{CBHLS}}\left(f\right)$, which functions as the audible heartbeat of the domain. In a young domain, this background manifests as a persistent high-frequency hiss with sharp pops, driven by the chaotic, frequent mergers of stellar-mass remnants. However, as the domain matures and the black hole population consolidates, this tone shifts. By the geriatric phase, the signal evolves into a gentle hiss with infrequent ultra-low-frequency rumble, dominated by the rare, distinct coalescences of hypermassive giants. Consequently, the measured spectral slope of $\Omega_{\mathrm{GW}}\left(f\right)$ serves as an independent chronometer; by resolving the dominant pitch of the background, we can directly constrain the Lattice Age τ of our local domain.

10. Experimental Tests and Falsifiability

This theory provides distinct and falsifiable experimental protocols.

- **Step 1: Map the Density Differential.** A lattice of ultra-stable optical clocks can map the local **Lattice Strain** by direct frequency comparison. Since frequency determines the local rate of time flow, the fractional frequency shift yields the normalized time-density differential:

$$\frac{\nu_A - \nu_B}{\nu_B} \approx \frac{\Delta\hat{t}}{\hat{t}}. \tag{28}$$

Critically, to decouple this signal from standard background redshift, the differential is calibrated using a local empirical circulating mass, allowing us to isolate the dynamic response of the time-density field from the static metric.

- **Step 2: Map the Spatial Metric.** An independent interferometric network

(such as LISA or a ground-based equivalent) measures the purely spatial geometry (g_{rr}).

- **Decision Logic:** If the measured spatial curvature (g_{rr}) is found to be a dependent function of the measured time-density differential ($\Delta\hat{t}$), the hypothesis that gravity is Density Pressure is supported. Conversely, if g_{rr} acts independently of the lattice strain, the Timeon framework is falsified.

Test 2: Secular Mass Drift via Einstein-Star Bifurcation

The central claim of the Timeon Lattice framework is that the Chrono-Quantum Mirror (CQM) suppresses Hawking evaporation, while Chrono-Emergence (CE) drives a positive secular drift in the black hole mass parameter ($\dot{M} > 0$). This contradicts the standard evaporative paradigm. We propose detecting this positive mass evolution by monitoring the angular and temporal separations of lensed stellar or pulsar sources—termed *Einstein-star bifurcation artifacts*.

For a Schwarzschild lens, the Einstein radius θ_E is given by

$$\theta_E = \sqrt{\frac{4GM}{c^2}\frac{D_{LS}}{D_L D_S}}, \tag{29}$$

where D_L, D_S, and D_{LS} are the angular diameter distances to the lens, source, and lens-source separation, respectively. A slow variation in $M(t)$ driven by internal fertility directly alters the lensing geometry. The measurable fractional change in angular separation scales as half the fractional mass change:

$$\frac{\dot{\theta}_E}{\theta_E} = \frac{1}{2}\frac{\dot{M}}{M}. \tag{30}$$

Observational campaigns monitoring isolated, mature black holes over 1 - 20 year baselines could resolve this minute expansion, confirming that internal volume generation supplants evaporation.

Additionally, variable sources (such as pulsars) aligned behind the lens experience a differential Shapiro delay:

$$\Delta t_{\text{delay}} \approx \frac{4GM}{c^3}\ln\left(\frac{r_1}{r_2}\right), \tag{31}$$

which scales linearly with M. Monitoring the drift in $\Delta t_{\text{delay}}(t)$ provides an independent, clock-based metric to quantify the rate of internal inflation ($\dot{M}$), validating the generative nature of the atomic phase within the horizon.

- **Method:** Use sophisticated space-based interferometry (existing and future instruments) to monitor an isolated, quiescent black hole.
- **Signal:** The target is a gravitationally lensed background star or star pair (an Einstein star pair).
- **Measurement:** By measuring the exact change in the lensed light's path over several years, we can detect a change in the black hole's mass (i.e., its spacetime curvature).
- **Decision Logic:** If an isolated black hole's mass is observed to increase (get fat)

over time, however slightly, this would be powerful evidence for the fertility hypothesis (CE) and a refutation of the evaporation-only paradigm. If it remains static or decreases, this specific prediction is falsified.

11. Results, Discussion, and Outlook

11.1. Unified Results

The construction satisfies: exact mirror first law; Petz ≥0.98; local GSL; Kerr calibration with no echoes and GR-like Love/heating; no divergences (log-only regulators); and a cosmological model where LGS (dark matter) and CSE-momentum (dark energy) arise as emergent lattice effects.

11.2. Finite-Diamond Algebra and Discussion

With $\left(\mathcal{A}_{\text{bulk}}, \mathcal{A}_{\text{edge}}, \tilde{\Omega}\right)$ and $\left[\hat{q}_A, \hat{p}^B\right] = i\delta_A^B \mathrm{e}^{-\Delta S_{\text{cap}}}$, the theory is finite. This framework supplants the standard evaporation ideology, rooted in concepts of black hole entropy and radiation. The CQM, by its very definition, is a finite time-density phase boundary at $\hat{t}_{\text{crit}}$ that suppresses black body radiation by preventing Planck-equilibrated emission. By removing this primary mass-loss channel, the theory ensures the dominant long-term dynamic is not decay, but the CE-driven accumulation of matter and the inevitable, rapid mergers that lead to the cyclical Chrono-Shear Event.

This framework suggests a distinct physical architecture: mass (e.g., a quark) represents a stable, localized *structural configuration* of Timeons. Rather than existing in an unobservable dimension, these quanta constitute the fundamental sub-Planckian substrate of the manifold itself. This lattice density performs two critical functions. Its passive role is to induce strain on the surrounding vacuum, generating the $\nabla\hat{t}$ gradient perceived as gravity. Its active role, as introduced in Section III.C, is to function as a reservoir of lattice tension. When the topological confinement of the particle is breached (e.g., nuclear fission), the Timeons catalyze the relaxation of this density, releasing the stored lattice binding energy as radiant output.

This unifies gravity (time pulling time) and $E = mc^2$ (time catalyzing energy) under the single DTD framework.

11.3. Predictions

No detectable echoes for $G(\omega) < 10^{-3}$; a stochastic background from the multiverse lattice; an effective dark sector (LGS) that may exhibit large-scale anisotropy; and a measurable, slow mass gain in isolated black holes.

11.4. Future Work

Future work will provide a comprehensive and definitive treatment of the Algebraic Operator Theory and Symplectic Geometry required to calculate the absolute phase-space of the Timeon field. This forthcoming monograph, the third installment in this series, details the formal derivation of the CET mechanism. Sub-

sequent research will focus on quantizing the causal regulator, exploring a cutoff holographic dual, and initiating lattice-diamond simulations to further map the T-Lattice dynamics.

12. Conclusion

$$\boxed{\tilde{\Omega}_{\text{bulk}} + \tilde{\Omega}_{\text{edge}} = 0,\ \ \delta Q_F = \left(\tilde{K}/c^2\right)\delta FA,\ \ \mathrm{d}S_{\text{gen}}/\mathrm{d}u \geq 0} \tag{32}$$

A unitary, thermodynamically closed quantum gravity emerges when emergence (CE) and Discrete-State Time Density (DTD) are embedded in finite causal diamonds. The dense-time phase, its finite threshold $\hat{t}_{\text{crit}}$, and the associated Chrono-Quantum Mirror together supply a single mechanism for wave suppression, black body failure, no-echo Kerr behavior, and domain-to-domain recycling, where the Chrono-Shear Event's extreme time-density phase amplifies the CE yield that seeds the next causal onset phase.

Acknowledgements

The author acknowledges the conceptual heritage of GR, quantum information theory, and thermodynamics that inspired the CE/DTD framework, including the Chrono-Quantum Mirror, the Chrono-Shear Event, and the finite-diamond lattice model. This work engages directly with the profound questions regarding black hole thermodynamics and information flow first rigorously posed by pioneers like Bekenstein [9] and Hawking [10].

Conflicts of Interest

The author declares no conflicts of interest regarding the publication of this paper.

References

[1] Davey, G. (2026) Universum Probabile Altera. *Journal of High Energy Physics, Gravitation and Cosmology*, **12**, 126-137. https://doi.org/10.4236/jhepgc.2026.121007

[2] Ashtekar, A. and Lewandowski, J. (2004) Background Independent Quantum Gravity: A Status Report. *Classical and Quantum Gravity*, **21**, R53-R152. https://doi.org/10.1088/0264-9381/21/15/r01

[3] Esaki, L. (1974) Long Journey into Tunneling. *Science*, **183**, 1149-1155. https://doi.org/10.1126/science.183.4130.1149

[4] Petz, D. (1986) Sufficient Subalgebras and the Relative Entropy of States of a Von Neumann Algebra. *Communications in Mathematical Physics*, **105**, 123-131. https://doi.org/10.1007/bf01212345

[5] Jacobson, T. (1995) Thermodynamics of Spacetime: The Einstein Equation of State. *Physical Review Letters*, **75**, 1260-1263. https://doi.org/10.1103/physrevlett.75.1260

[6] Berti, E., Cardoso, V. and Starinets, A.O. (2009) Quasinormal Modes of Black Holes and Black Branes. *Classical and Quantum Gravity*, **26**, Article ID: 163001. https://doi.org/10.1088/0264-9381/26/16/163001

[7] Vaz, C. (2014) Black Holes as Gravitational Atoms. *International Journal of Modern Physics D*, **23**, Article ID: 1441002.

https://doi.org/10.1142/s0218271814410028

[8] Corda, C. (2023) Schrödinger and Klein-Gordon Theories of Black Holes from the Quantization of the Oppenheimer and Snyder Gravitational Collapse. *Communications in Theoretical Physics*, **75**, Article ID: 095405. https://doi.org/10.1088/1572-9494/ace4b2

[9] Bekenstein, J.D. (1973) Black Holes and Entropy. *Physical Review D*, **7**, 2333-2346. https://doi.org/10.1103/physrevd.7.2333

[10] Hawking, S.W. (1975) Particle Creation by Black Holes. *Communications in Mathematical Physics*, **43**, 199-220. https://doi.org/10.1007/bf02345020

[11] Wald, R.M. (1984) General Relativity. University of Chicago Press. https://doi.org/10.7208/chicago/9780226870373.001.0001

Appendix A. Einstein Limit Recovery

In the low-$\hat{t}$ limit $\hat{t}\to 1$ and $F(\hat{t})\to 0$, CE contributions vanish and

$$G_{\mu\nu}=8\pi G\langle T_{\mu\nu}\rangle$$

is recovered identically (cf. [11]), ensuring compatibility with classical GR tests. This $\hat{t}\to 1$ limit corresponds to the stable wave phase of the DTD field, in which spacetime supports quantum coherence, tunneling, and black body radiation.

Appendix B. Numerical Support for the Chrono-Emergent Multiverse

We summarize quantitative elements of the discrete, three-state time-density cosmology. All figures were generated with Python (NumPy, Matplotlib). Canonical parameters: $\hat{t}_{\text{vac}}=1$, $R=50$, $f_{\text{BH}}=0.02$, $\tau=\text{Gyr}$, $p=2$, $A_S=3\times 10^{-3}$, $\phi=0.2$, $N=10^7$, $f_{\text{dark}}=0.27$.

B.1. Temporal-Density Parameterization

We normalize the vacuum time density to $\hat{t}_{\text{vac}}=1$ ($\hat{t}_1$) and define the dense-time (black-hole) density as $R\hat{t}_{\text{vac}}$ with $R=50$. For a dense-time fraction f_{BH}, the mean temporal density is

$$\hat{t}_{\text{avg}}=(1-f_{\text{BH}})\hat{t}_{\text{vac}}+f_{\text{BH}}\left(R\hat{t}_{\text{vac}}\right). \tag{33}$$

Figure A1 shows $\hat{t}_{\text{avg}}$ (denoted as ρ_{avg} in plots) vs. f_{BH}.

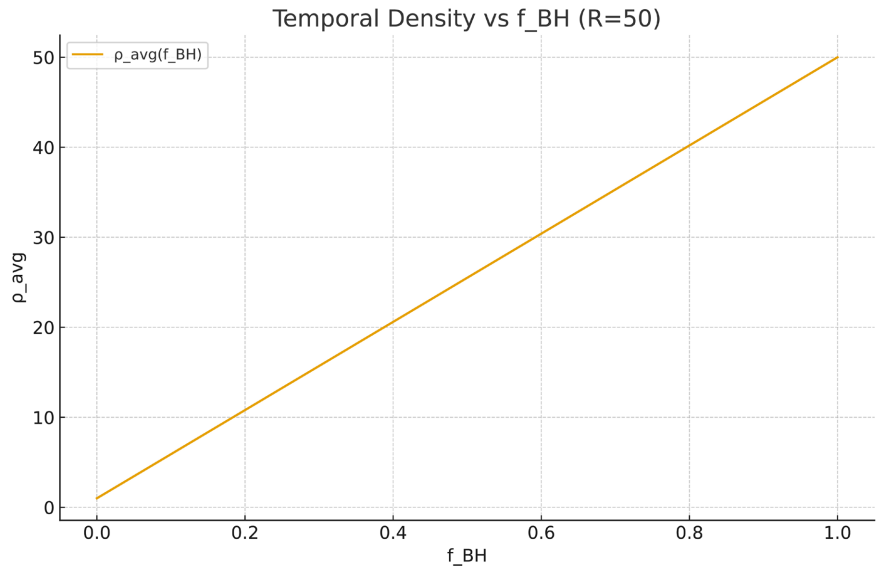

Figure A1. Mean temporal density versus dense-time fraction f_{BH} with $R=50$. Present-epoch anchor: $f_{\text{BH}}=0.02$.

B.2. Ensemble-Average Chronodynamic Diffusivity

Time density is discrete, with phases $\hat{t}_1$ (Vacuum), $\hat{t}_3$ (Shear), and $\hat{t}_2$ (Dense).

We model between-state activity via a transition matrix $\boldsymbol{K}_t$ with off-diagonal entries k_{ij} (probability per Gyr). These transitions drive the cyclical evolution between the causal onset and the lattice apogee.

B.3. Temporal Damping Coefficients

Within-state perturbations are modeled to relax exponentially, $\delta\hat{t}_i(\tau) = \delta\hat{t}_i(0)\mathrm{e}^{-\beta_i\tau}$. Reflecting the hierarchy of lattice saturation, the theoretical damping coefficients follow the ordering $\hat{t}_3 > \hat{t}_2 > \hat{t}_1$. This ensures that the Shear Phase (Big Bang/Deconfinement) and Dense Phase (Black Hole) exhibit rapid coherence suppression compared to the vacuum state.

B.4. Black-Body Failure and Spectral Suppression

We modify Planck's law by a chronodynamic factor $S_\beta(x) = \exp\left(-\beta x^p\right)$ with $p = 2$:

$$B_\beta(x) = \frac{x^3}{\mathrm{e}^x - 1}\exp\left(-\beta x^2\right), \quad x = \frac{h\nu}{kT}. \tag{34}$$

Figure A2 shows this suppression. Consistent with the density hierarchy ($\hat{t}_3 > \hat{t}_2 > \hat{t}_1$), the Dense Phase $\hat{t}_2$ exhibits critical suppression ($\beta \to$ large), effectively quenching the spectrum. This justifies the CQM's **Black Body Failure**, wherein the region becomes radiatively dark rather than emitting a thermal Hawking spectrum.

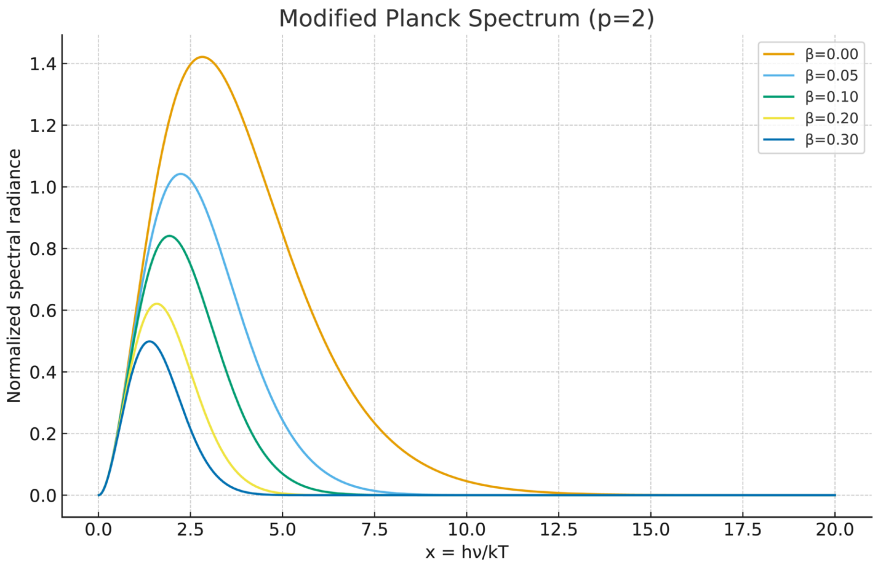

Figure A2. Modified black-body spectra with chronodynamic suppression. $\beta = 0$ recovers Planck; larger β trims the high-frequency tail, simulating the onset of the dense-time phase.

B.5. Chrono-Shear Burst Statistics

Simulated shear fluctuations ($\hat{t}_3$) are brief and localized. Figure A3 shows an ensemble of simulated bursts.

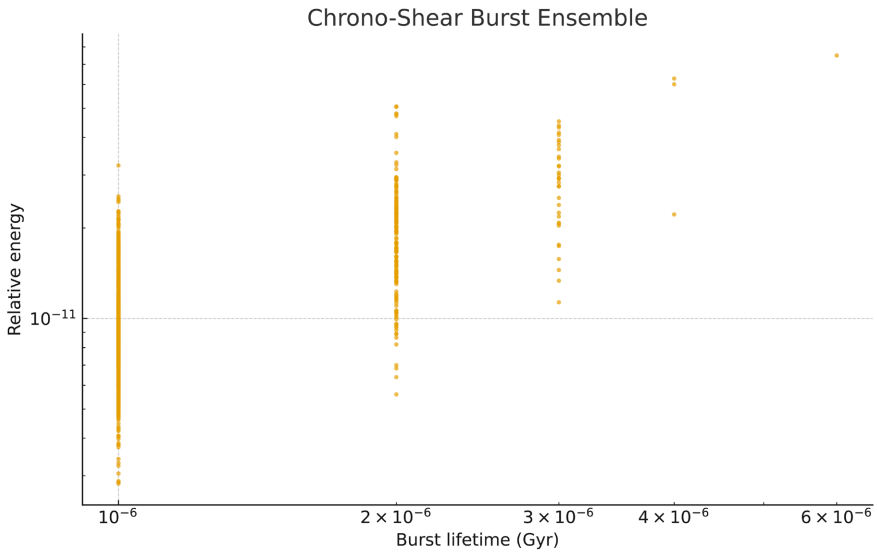

Figure A3. Simulated shear bursts: lifetime (in Gyr) vs. relative energy.

B.6. Multiverse Lattice Coupling

Let d_{eff} be the effective neighbor degree and ζ the per-link bleed coupling. Matching a dark-sector fraction f_{dark} yields $\zeta \approx f_{\text{dark}}/d_{\text{eff}}$. **Figure A4** maps feasible (d_{eff}, ζ) pairs for $f_{\text{dark}} \approx 0.27$.

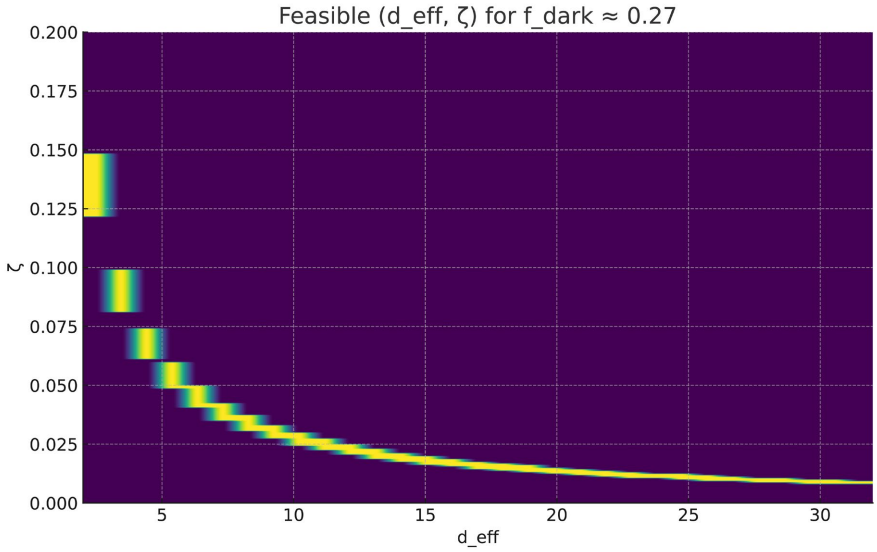

Figure A4. Feasible (d_{eff}, ζ) combinations where ζd_{eff} matches $f_{\text{dark}} \approx 0.27$ within ±10%.